Adjusted Normalized Emissivity Method for surface temperature and emissivity retrieval from optical and thermal infrared remote sensing data

César Coll, Enric Valor, Vicente Caselles, and Raquel Niclòs

Department of Thermodynamics, Faculty of Physics, University of Valencia, Valencia, Spain

[1] A methodology for the retrieval of surface temperatures and emissivities combining visible, near infrared and thermal infrared remote sensing data was applied to Digital Airborne Imaging Spectrometer (DAIS) data and validated with coincident ground measurements acquired in a multiyear experiment held in an agricultural site in Barrax, Spain. The Adjusted Normalized Emissivity Method (ANEM) is based on the use of visible and near infrared data to estimate the vegetation cover and model the maximum emissivity according to the Vegetation Cover Method. The pixel-dependent maximum emissivity is used as the initial guess of the Normalized Emissivity Method to obtain the surface temperature and emissivity from the thermal infrared data. ANEM allows adjusting the initial emissivity with regard to the spatial variation of emissivity with vegetation cover, instead of using a fixed emissivity. Surface temperatures derived with ANEM agreed well with ground data, with a standard deviation of ±0.8 K and nearly zero bias for all the surface types. Retrieved emissivities were mostly within ±0.01 of the measured values, despite certain instrumental problems apparent in the thermal part of DAIS. An analysis of the emissivity spectra was performed, showing the utility in the discrimination of different agricultural surface types in the area.   *INDEX TERMS:* 0933 Exploration Geophysics: Remote sensing; 1640 Global Change: Remote sensing; 1694 Global Change: Instruments and techniques; 3360 Meteorology and Atmospheric Dynamics: Remote sensing; *KEYWORDS:* thermal infrared, surface temperature, emissivity

1.   Introduction

[2] Land surface temperature and emissivity are key parameters in the determination of the radiation balance at the surface, and are necessary for meteorological and climate models, lithological mapping and resources exploration. The retrieval of temperature and emissivity from thermal infrared remote sensing measurements is a challenging problem. First, at-sensor radiance data must be corrected for atmospheric effects, which depend on the vertical distribution of absorbing and emitting gases (mainly water vapor). Second, temperature and emissivity are coupled in the thermal radiances and thus measurements are underdetermined: for N spectral channels there will be always N+1 unknowns (surface temperature and N channel emissivities). In order to break down the indeterminacy, additional hypotheses usually based on emissivity measurements or models are required. A number of temperature-emissivity separation algorithms for multispectral thermal infrared data have been proposed [*Gillespie*, 1986; *Becker and Li*, 1990; *Kealy and*

Hook, 1993; *Gillespie et al.*, 1998]. Revisions and intercomparison of different methods have been recently published [*Caselles et al.*, 1997; *Li et al.*, 1999; *Dash et al.*, 2002].

[3] The objective of the present paper is to propose an Adjusted Normalized Emissivity Method (ANEM) to separate temperature and emissivity. The approach is based on the use of visible and near infrared data to infer the vegetation cover of the land surface and model the maximum channel emissivity using the Vegetation Cover Method (VCM) proposed by *Valor and Caselles* [1996]. Then, the pixel-dependent maximum emissivity is used as an input of the Normalized Emissivity Method (NEM) [*Gillespie*, 1986] to retrieve the surface temperature and the channel emissivities. ANEM was first used by *Coll et al.* [2001a], where maximum emissivity values obtained from ground measurements were used in some test fields. In the present paper, ANEM is made operational by using the VCM to calculate the maximum emissivity independent of ground data. The algorithm was applied to a series of Digital Airborne Imaging Spectrometer (DAIS) scenes recorded in the Digital Airborne Imaging Spectrometer Experiment (DAISEX), a three-year experiment with coincident atmospheric and

Table 1. Center Wavelength (CW) and Full Width at Half Maximum (FWHM) of Digital Airborne Imaging Spectrometer (DAIS) Channels 74–79

Channel	CW (μm)	FWHM (μm)
74	8.75	0.85
75	9.65	0.88
76	10.48	0.92
77	11.27	1.07
78	12.00	1.38
79	12.67	1.54

ground measurements carried out in an agricultural site in Barrax, Spain in 1998–2000. The ANEM derived temperatures and emissivities were validated with ground data measured in selected sites. An analysis of the emissivity spectra retrieved for the different types of surface present in the area was also performed.

[4] The article follows with a description of the experimental data set used in this study. Next, the pre-processing of the DAIS thermal infrared images is addressed, including the atmospheric correction and the calibration. In section 4, the ANEM algorithm is briefly described. Section 5 shows the results obtained. Finally, the main conclusions of the work are summarized.

2. Experimental Data Set

[5] DAISEX was supported by the European Space Agency (ESA) to demonstrate the operational retrieval of bio/geophysical variables from spectrometer data and to validate the requirements for future space-borne instruments [*Berger et al.*, 2001; *European Space Agency*, 2001]. The experimental campaigns were held in the test site of Barrax (39°3′N, 2°6′W, and 700 m over sea level), an agricultural site in the La Mancha region, close to the city of Albacete, Spain. The area was cultivated with both dry (barley) and irrigated crops (corn, barley, wheat and alfalfa). The three field campaigns were carried out in August 11, 1998; June 3 and 4, 1999; and June 29, 2000, thus covering different stages of crop development. For each campaign, extensive data sets of airborne images and ground based measurements of atmospheric and surface properties were collected. The data sets and accompanying documentation are currently available to the public at http://io.uv.es/projects/daisex/, together with details on the test site and the campaigns. A description of the data relevant to this paper follows.

2.1. Digital Airborne Imaging Spectrometer Data

[6] DAIS is a 79-channel scanner operated by the German Aerospace Center (DLR), which covers the range from 0.5 μm to 14 μm. Channels 74–79 are located in the thermal infrared region (see Table 1). DAIS scans ±26° with an instantaneous field of view of 3.3 mrad, yielding a spatial resolution of 5 m at nadir from an altitude of 3050 m above ground level. For more details on DAIS see *Müller et al.* [2001]. Table 2 lists the DAIS scenes acquired during the DAISEX campaigns. For each flight, two consecutive lines of data were recorded with short time lag. In the 1998 and 1999 campaigns, line 1 was in the North-South direction and line 2 was in the East-West direction, both lines overlapping on a 3 km × 3 km area of the Barrax test site. In the 2000 campaign, both lines were in the East-West direction,

with line 2 displaced to the South but overlapping part of line 1. Flights were usually done around local solar noon, except for the morning and afternoon flights on June 4, 1999.

[7] All DAIS lines were geometrically corrected and geocoded by DLR using a parametric approach [*Hausold*, 2001]. In order to check the quality of the geocoding, the positions of several ground control points in the areas where scenes overlapped were compared for each flight. An average deviation of ±2 pixels was found. The thermal channels of DAIS were calibrated in the laboratory with two blackbodies at different temperatures [*Strobl et al.*, 1997]. Data were given as digital counts (DC) convertible to radiances, with 1 DC = 10^{-7}Wcm^{-2}sr^{-1}μm^{-1} for channels 74–79. However, the Kennedy scan mechanism used by DAIS makes that the signal at the detector is contaminated by a considerable fraction of intrinsic background radiation. This results in inaccurate laboratory calibration, as noticed in previous DAIS campaigns [*Strobl and Zhukov*, 1998; *Coll et al.*, 2001a, 2001b]. Calibration errors are scene-dependent and cannot be predicted. Therefore a vicarious calibration is required for each DAIS scene, which is described in section 3.2.

2.2. Temperature Measurements

[8] In the DAISEX campaigns, radiometric temperatures were measured in various selected fields concurrently to each DAIS image acquisition. The water body located in the test area and one site of bare soil were taken as calibration targets since they covered the temperature range of the area. In addition, other fields (corn, alfalfa, barley, grass, and bare soil, depending on the year) were selected as validation sites for the DAIS retrieved temperatures and emissivities.

[9] Temperatures were measured with the four-channel CIMEL thermal infrared radiometer CE 312 (channels 1 to 4 at 8–13 μm; 11.5–12.5 μm; 10.5–11.5 μm; and 8.2–9.2 μm, respectively), and two Everest thermometers (models 210 and 112.2 L) working in the 8–13 μm band. (The use of company and brand names is for information only and does not imply endorsement by the authors.) The CE 312 radiometer is provided with an internal radiance reference for compensating the cavity radiance at the detector. A detailed description of the instrument is given by *Sicard et al.* [1999]. Its calibration was checked in the laboratory and in the field during the campaigns using a portable blackbody calibration source (Everest model 1000). According to this, an accuracy of ±0.1 K with no bias was obtained for the four CE 312 channels.

Table 2. DAIS Flights in the Digital Airborne Imaging Spectrometer Experiment (DAISEX) Campaigns With the Date and Time of Pass Over the Barrax Test Site

Campaign	Date	Local Solar Time	
		Line 1	Line 2
1998	August 11	12:10	12:26
1999	June 3	11:52	12:08
1999	June 4	8:01	8:16
1999	June 4	14:58	15:11
2000	June 29	12:12	12:23

Table 3. Surface Temperatures (Emissivity Corrected) Measured Coincidentally With DAIS for the Selected Fields[a]

Date	Field	Type	Line 1 T (°C)	Line 1 σ_T(K)	Line 2 T (°C)	Line 2 σ_T(K)
August 11, 1998	W1*	water	21.9	0.9	21.9	0.9
	S3*	bare soil	52.6	0.6	54.7	0.8
	C5	corn	28.5	0.3	29.1	0.3
	A4	alfalfa	27.6	1.6	27.1	1.1
	S1	bare soil	54.4	1.5	56.2	1.3
June 3, 1999	W1*	water	22.7	0.4	22.7	0.4
	S10*	bare soil	48.9	1.0	50.5	1.0
	B27	non irr. barley	39.6	3.0	42.9	5.2
	S10b	bare soil	49.2	1.7	50.1	1.2
June 4, 1999 (morning)	W1*	water	19.5	0.4	19.5	0.4
	S10*	bare soil	30.0	0.9	33.5	1.8
	B27	non irr. barley	24.8	1.8	25.4	1.2
	B25	non irr. barley	25.3	1.2	25.1	1.4
June 4, 1999 (afternoon)	W1*	water	20.9	0.6	20.9	0.6
	S10*	bare soil	50.2	1.2	48.2	0.7
	B27	non irr. barley	39.7	1.9	40.3	3.5
	S10b	bare soil	47.5	1.4	48.1	1.4
June 29, 2000	W1*	water	21.5	0.5	21.5	0.5
	S6*	bare soil	59.1	1.4	61.4	1.4
	S5	bare soil	58.4	2.4	61.3	2.6
	G20	grass	39.9	2.8	41.3	1.9

[a]The asterisk means calibration target. The uncertainty σ_T associated with each temperature measurement is given.

Everest thermometers were calibrated against the calibration source and compared with CE 312 channel 1 (with similar band-pass) for several reference surfaces in the field. These instruments showed large deviations (up to 3 K) depending on the source temperature and the ambient operating temperature, and dispersions of about ±1 K. For this reason, calibration equations were derived for the two Everest thermometers taking the calibration source and the CE 312 temperatures as a reference. In this way, we could correct for systematic deviations in radiometric temperatures; however the (absolute) accuracy was still limited to ±1.0 K for the two Everest instruments. Taking into account the greater accuracy of channel 1 of CE 312, it was used for the bare soil calibration site. For the water body calibration site, we used conventional contact thermometers (accuracy of ±0.1 K) immersed at the top layer of water (1–2 cm) in order to minimize the possible difference between radiant surface temperatures and bulk temperatures. In the 1999 and 2000 campaigns, we also performed radiometric measurements to check that this difference was negligible.

[10] Radiometric temperatures were sampled along transects marked with Global Positioning System coordinates, so it was possible to identify the pixel corresponding to the site of the measurement at the time of the DAIS overpass with an accuracy of about 1 m. For each site, the ground temperatures measured within ±2 min around the overpass time were averaged and the standard deviation was calculated to evaluate the temperature variability. Then, the average radiometric temperatures were corrected for surface emissivity effects, including the reflection of sky irradiance. To this end, the downward hemispherical sky radiance was measured regularly during the temperature transects and surface emissivity measurements were performed in the 8–13 μm band for the different fields (see section 2.3).

[11] Table 3 shows the database of ground temperatures coincident with the DAIS flights for the three DAISEX campaigns. Together with the mean surface temperature, we give the uncertainty in the measurement, due to the instrument inaccuracy, the spatial variability of the ground temperatures, and the error in the emissivity correction (except for the water temperatures). The largest source of uncertainty was usually the natural spatial variation of temperature within a field, especially for incomplete canopies with large differences between soil and vegetation temperatures (e.g., non-irrigated barley).

2.3. Emissivity Measurements

[12] Emissivity measurements were performed in the four channels of the CE 312 radiometer for various surfaces of the area. Emissivities in channel 1 (8–13 μm) were required to derive surface temperatures from measured at-surface radiances. On the other hand, measurements in the narrow channels of CE 312 (channels 2–4) were useful to assess the spectral variation of emissivity and to compare with DAIS derived emissivities. Channel 4 of CE 312 (8.2–9.2 μm) is similar to DAIS channel 74, and channels 3 and 2 of CE 312 (10.5–11.5 μm and 11.5–12.5 μm, respectively) cover the spectral range of DAIS channels 76–78. Measurements were carried out with the box method (see *Rubio et al.* [1997] for details). More than 15 measurements were done for each sample and channel, the mean value and the standard deviation being given in Table 4. Measurements were taken in the laboratory for soils and in the field for crops. Measurements for soils were quite accurate (between ±0.2% and ±0.7%) due to laboratory stable conditions. Measurements for crops in the field had an error between ±0.5% and ±1.4%.

3. Preprocessing of DAIS Thermal Data

[13] Temperature-emissivity separation algorithms require the atmospheric correction of at-sensor radiances. Additionally, the DAIS thermal channels require ground cali-

Table 4. Emissivity Measurements in the CE 312 Channels for Various Fields in the DAISEX Campaigns

| Campaign	Field	Type	Ch. 1, 8–13 μm	Ch. 4, 8.2–9.2 μm	Ch. 3, 10.5–11.5 μm	Ch. 2, 11.5–12.5 μm
1998	S3	bare soil	0.966 ± 0.003	0.959 ± 0.006	0.968 ± 0.005	0.965 ± 0.004
	C5	corn	0.992 ± 0.005	0.992 ± 0.005	0.992 ± 0.005	0.992 ± 0.005
	A4	alfalfa	0.980 ± 0.006	0.981 ± 0.007	0.978 ± 0.009	0.981 ± 0.007
	S1	bare soil	0.960 ± 0.002	0.944 ± 0.007	0.963 ± 0.004	0.963 ± 0.006
1999	S10	bare soil	0.966 ± 0.003	0.955 ± 0.005	0.969 ± 0.002	0.967 ± 0.005
	B27	non irr. barley	0.971 ± 0.006	–	–	–
2000	S6	bare soil	0.960 ± 0.005	0.949 ± 0.003	0.964 ± 0.002	0.964 ± 0.002
	G20	grass	0.981 ± 0.007	0.977 ± 0.014	0.974 ± 0.009	0.973 ± 0.008
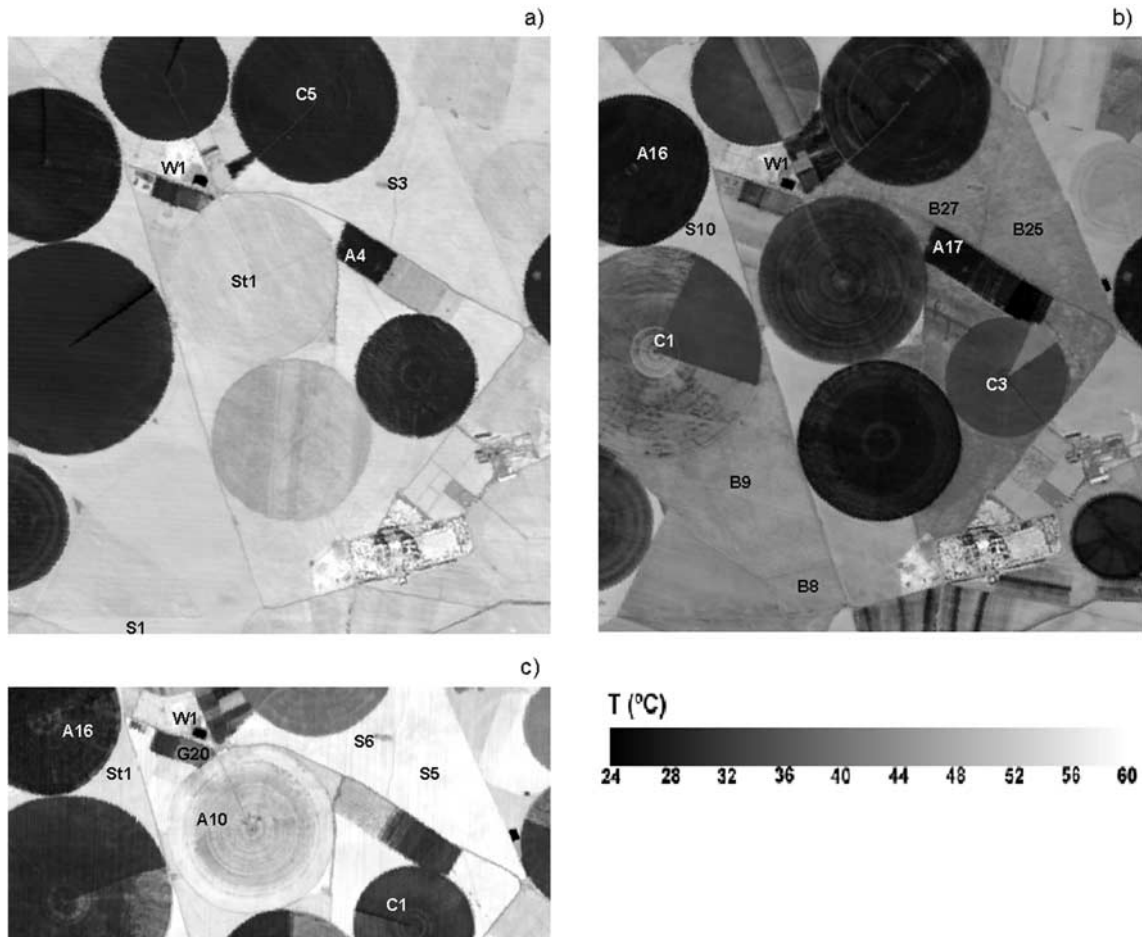
Figure 1. Images of surface temperature derived from line 1 of the DAIS flights on (a) August 11, 1998; (b) June 3, 1999; and (c) June 29, 2000. Selected fields are indicated in the images (W, water; S, bare soil; St, stubble; C, corn; A, alfalfa; B, non-irrigated barley; G, grass.)

bration as discussed in section 2.1. In this section we describe both processes, the overall goal of which is to convert at-sensor, laboratory-calibrated radiances into at-surface, ground-calibrated radiances.

3.1. Atmospheric Correction

[14] DAIS images were atmospherically corrected by DLR using the ATCOR4 model [*Richter*, 2000]. For the thermal infrared channel j, at-surface radiances, L_j^{surf}, can be obtained from at-sensor radiances, L_j^{sens}, according to

$$L_j^{surf} = \frac{L_j^{sens} - L_j^{atm}(\theta)}{\tau_j(\theta)} \qquad (1)$$

where θ is the scan angle, τ_j is the atmospheric transmittance, and L_j^{atm} is the path radiance. The ATCOR4 model calculates the atmospheric parameters τ_j and L_j^{atm} with the MODTRAN4 radiative transfer code [*Berk et al.*, 1999] and vertical atmospheric profiles. For the DAISEX campaigns, local radiosonde measurements of pressure, temperature, humidity, and ozone abundance were used. Radiosondes were launched from the Barrax test site one hour before and one hour after each DAIS flight.

[15] The use of channel integrated atmospheric parameters (τ_j and L_j^{atm}) introduces inherent errors in the retrieval of surface emissivities and temperatures, which are due to the approximations required in the resampling of monochromatic radiative transfer calculations with the spectral response function of the channel. This effect was investigated by *Richter and Coll* [2002] for different sensors with channels from 8 to 14 µm, showing that it was larger for broadband channels with low atmospheric transmittance. For DAIS channel 79, errors introduced in retrieved emissivity were up to ±2%, while for the other DAIS channels they were about ±0.5%. For this reason, only channels 74–78 (8.5 to 12.5 µm) were used in the present study.

3.2. Vicarious Calibration

[16] The methodology followed for the vicarious calibration of DAIS thermal channels was described by *Coll et al.* [2001a], where the two scenes of the 1998 campaign were analyzed. In the present study, we extended the calibration to the 1999 and 2000 scenes. The field measurements of temperature and emissivity for the two calibration targets (bare soil and water) were used to calculate the at-surface radiances, including the reflection of the downwelling sky
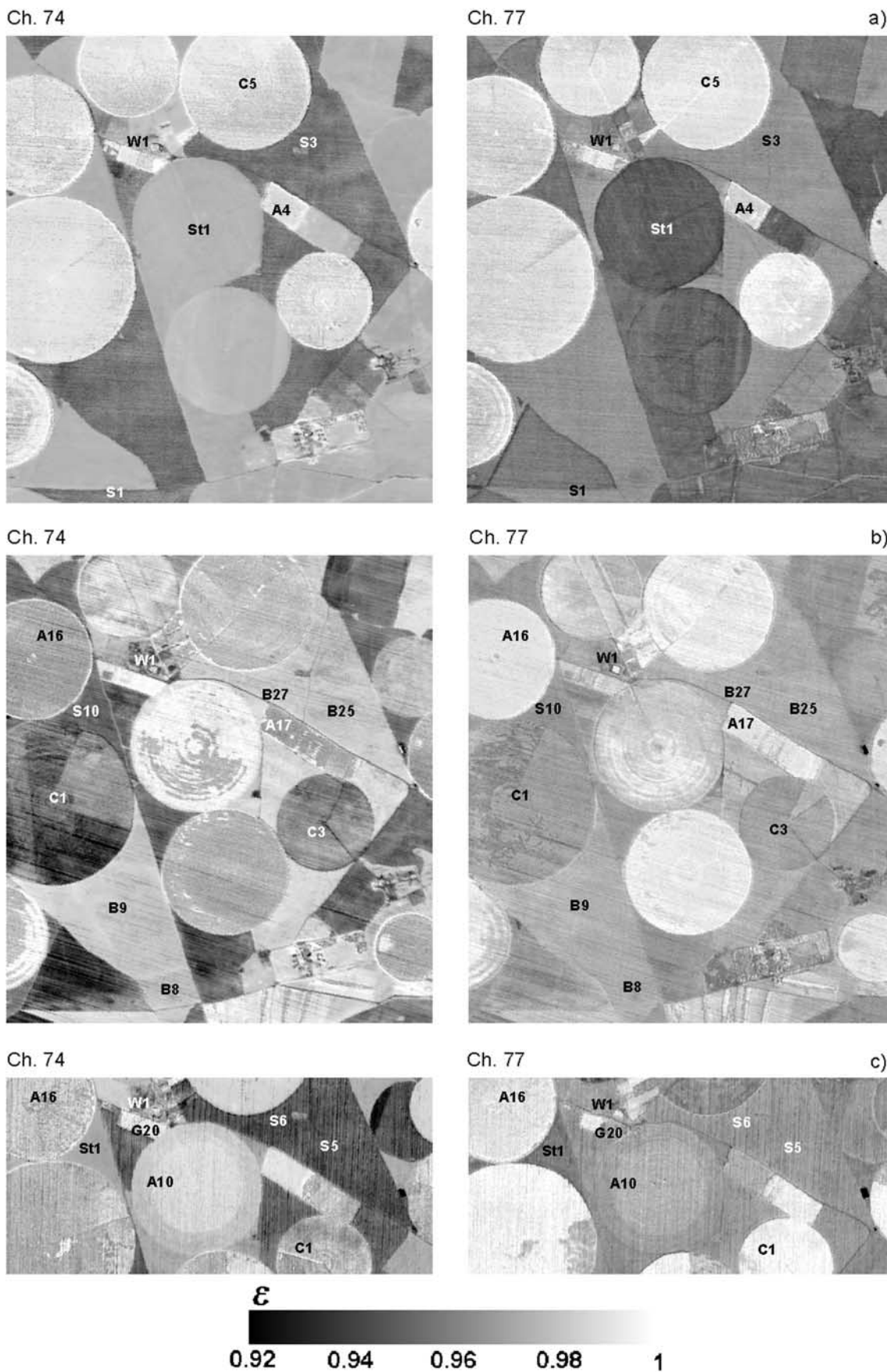
Figure 2. Images of emissivity in channels 74 and 77 derived from line 1 of the DAIS flights on (a) August 11, 1998; (b) June 3, 1999; and (c) June 29, 2000. Selected fields are indicated as in Figure 1.

Table 5. Surface Temperatures Derived From DAIS Data With the Adjusted Normalized Emissivity Method (ANEM)[a]

Date	Field	Type	Line 1 T, °C	Line 1 σ_T, K	Line 1 ΔT, K	Line 2 T, °C	Line 2 σ_T, K	Line 2 ΔT, K
August 11, 1998	W1	water	22.7	0.4	−0.8	22.2	0.3	−0.3
	S3	bare soil	52.8	0.5	−0.2	54.9	0.3	−0.2
	C5	corn	28.3	0.1	0.2	29.2	0.2	−0.1
	A4	alfalfa	28.2	0.8	−0.6	27.9	0.3	−0.8
	S1	bare soil	54.2	0.6	0.2	54.3	0.3	1.9
June 3, 1999	W1	water	22.7	0.1	0.0	22.9	0.2	−0.2
	S10	bare soil	49.0	0.3	−0.1	50.7	0.1	−0.2
	B27	non irr. barley	39.2	0.2	0.4	44.6	0.6	−1.7
	S10b	bare soil	49.3	0.2	−0.1	50.2	0.2	−0.1
June 4, 1999 (morning)	W1	water	20.2	0.7	−0.7	19.9	0.5	−0.4
	S10	bare soil	30.0	0.1	0.0	33.5	0.2	0.0
	B27	non irr. barley	24.0	0.1	0.8	25.2	0.2	0.2
	B25	non irr. barley	24.2	0.2	1.1	25.8	0.2	−0.7
June 4, 1999 (afternoon)	W1	water	21.8	0.9	−0.9	20.9	0.1	0.0
	S10	bare soil	50.2	0.2	0.0	48.3	0.3	−0.1
	B27	non irr. barley	40.0	0.6	−0.3	38.7	0.5	1.6
	S10b	bare soil	49.8	0.2	−2.3	48.7	0.3	−0.6
June 29, 2000	W1	water	21.7	0.3	−0.2	22.3	0.4	−0.8
	S6	bare soil	58.6	0.4	0.5	60.4	0.3	1.0
	S5	bare soil	59.8	0.5	−1.4	60.9	0.3	0.4
	G20	grass	40.2	0.4	−0.3	41.8	0.6	−0.5

[a]σ_T is the standard deviation of the DAIS derived temperatures for the 5×5 pixels extracted for each field, and ΔT is the difference between the measured temperatures (Table 3) and the DAIS derived temperatures.

flux, which was estimated with the local radiosonde profiles and MODTRAN4. The comparison of the calculated and atmospherically corrected DAIS radiances resulted in large differences both in terms of amplitude and spectral shape, which were mainly attributed to errors in the laboratory calibration of DAIS. Taking the calculated radiances as a reference, a linear calibration equation was derived to obtain the at-surface, ground calibrated radiance $L_j^{surf}(c)$ from the original L_j^{surf} according to

$$L_j^{surf}(c) = G_j L_j^{surf} + N_j \qquad (2)$$

where calibration coefficients G_j and N_j depend on the channel and the scene, and were calculated for all the scenes of the DAISEX campaigns.

[17] The differences between the calculated and the original at-surface radiances may be affected by possible errors in the atmospheric correction, in addition to calibration errors. Because of the size and spectral dependence of the differences, and taking into account that we used local and near simultaneous atmospheric profiles, we believe that the most part of the discrepancies was caused by the calibration of the DAIS thermal channels. In any case, it should be noted that the overall goal of equations (1) and (2) (both linear in radiances) is to relate at-sensor DAIS radiances with at-surface radiances based on ground measurements. Therefore no matter the differences are due to the atmospheric correction or the calibration, the accuracy of the procedure depends ultimately on the quality of the ground temperatures and emissivities used for the at-surface radiance calculations. However, it is necessary to perform the atmospheric correction separately in order to account for angular effects due to the increase of atmospheric path length with scan angle ($\pm 26°$ for DAIS). If we assume that the atmosphere did not change much between consecutive lines of a given flight (15–

20 min) and was homogeneous over the test site (3×3 km^2), the impact of atmospheric correction errors is rather negligible.

4. The Adjusted Normalized Emissivity Method

[18] The calibrated, at-surface radiance, $L_j^{surf}(c)$, is related to the surface temperature, T, and the channel emissivity, ε_j, according to

$$L_j^{surf}(c) = \varepsilon_j B_j(T) + (1 - \varepsilon_j)\frac{F_j^{sky}}{\pi} \qquad (3)$$

where B_j is Planck's function weighted for channel j and F_j^{sky} is the downwelling sky irradiance (Lambertian reflection is assumed). Equation (3) is strictly true for homogeneous and isothermal surfaces; however, it can be used for mixed pixels (e.g., soil and vegetation) if T and ε_j are considered as the effective temperature and emissivity, respectively, which are defined from the temperatures and emissivities of the elements of the surface [*Caselles and Sobrino*, 1989; *Becker and Li*, 1995].

Table 6. Mean Value and Standard Deviation of ΔT (Measured Minus Retrieved Temperatures, in K), for Each Surface Type[a]

Surface Type	ANEM	NEM, $\varepsilon_{NEM} = 0.97$
Bare soil (18)	−0.1 ± 0.9	−0.1 ± 0.9
Non-irr. Barley (8)	0.2 ± 1.1	−0.6 ± 1.0
Green vegetation (6)	−0.1 ± 0.5	−1.4 ± 0.4
Water (10)	−0.4 ± 0.3	−1.3 ± 0.2
Total (42)	−0.1 ± 0.8	−0.7 ± 0.9

[a]The number of data points is indicated in parentheses next to each surface type.

Table 7. Differences in Channel Emissivities Retrieved for the Two Consecutive Lines of Each DAIS Flight[a]

Date	Ch. 74	Ch. 75	Ch. 76	Ch. 77	Ch. 78
August 11, 1998	-0.001 ± 0.007	-0.004 ± 0.006	0.001 ± 0.006	-0.001 ± 0.006	0.002 ± 0.009
June 3, 1999	-0.001 ± 0.009	-0.002 ± 0.008	0.002 ± 0.007	-0.002 ± 0.007	-0.003 ± 0.011
June 4, 1999 (morning)	0.005 ± 0.011	0.006 ± 0.014	0.001 ± 0.007	0.003 ± 0.010	0.000 ± 0.014
June 4, 1999 (afternoon)	0.003 ± 0.011	-0.001 ± 0.009	0.001 ± 0.007	-0.005 ± 0.008	-0.009 ± 0.012
June 29, 2000	-0.003 ± 0.009	-0.003 ± 0.007	0.001 ± 0.007	-0.002 ± 0.008	-0.001 ± 0.012

[a]The average value and the standard deviation of the differences for the area overlapped by the two lines are given.

[19] Equation (3) shows the coupling of temperature and emissivity in the emitted radiance, and of emissivity and atmospheric downwelling radiation in the reflection term. One of the simplest approaches to solve equation (3) for T and ε_j is the Normalized Emissivity Method (NEM) [*Gillespie*, 1986], where a constant emissivity value ε_{NEM} is assumed for all channels and pixels (e.g., $\varepsilon_{NEM} = 0.97$). Then, temperatures are inverted from equation (3) using an estimate of F_j^{sky}, and for each pixel, the maximum of the N channel temperatures is selected as the actual surface temperature. Finally, this temperature is used again in equation (3) to calculate the N channel emissivities, the assumed ε_{NEM} being always recovered for the channel with maximum temperature. NEM is a relative method: since ε_{NEM} is arbitrary, the retrieved temperature and emissivity spectrum may be biased while the spectral variation of emissivity is accurate.

[20] It can be easily seen that, for a given ε_{NEM}, the maximum temperature is obtained at the channel where the actual emissivity is the highest. Only in the case that the assumed ε_{NEM} matches the maximum emissivity of the surface, the retrieved temperature and emissivity will be correct. Inspection of published emissivity measurements (e.g., *Salisbury and D'Aria* [1992]; ASTER spectral library at http://speclib.jpl.nasa.gov) shows that maximum emissivities occur in the $10-12.5$ μm wave band for most natural surfaces, roughly ranging from 0.95 (exposed soils) to 0.99 (densely vegetated surfaces). For mixed surfaces, the maximum emissivity depends on the amount of the vegetation and its structure.

[21] The algorithm proposed in this paper retains the main features of NEM but allows a pixel-by-pixel adjustment of the initial ε_{NEM} accounting for the spatial variation of the vegetation cover. The so-called Adjusted Normalized Emissivity Method (ANEM) first calculates the maximum emissivity for each pixel using the Vegetation Cover Method (VCM) of *Valor and Caselles* [1996]. As detailed in Appendix A, the maximum emissivity in the DAIS thermal channels $74-78$ can be modeled as

$$\varepsilon_{max} = 0.988 P_v + 0.964(1 - P_v) + 0.06 P_v(1 - P_v) \quad (4)$$

where P_v is the vegetation fractional cover estimated from visible and near infrared remote sensing data. The method used to obtain P_v from DAIS data is also detailed in Appendix A. Equation (4) is not valid for water, for which the value $\varepsilon_{max} = 0.99$ can be selected according to
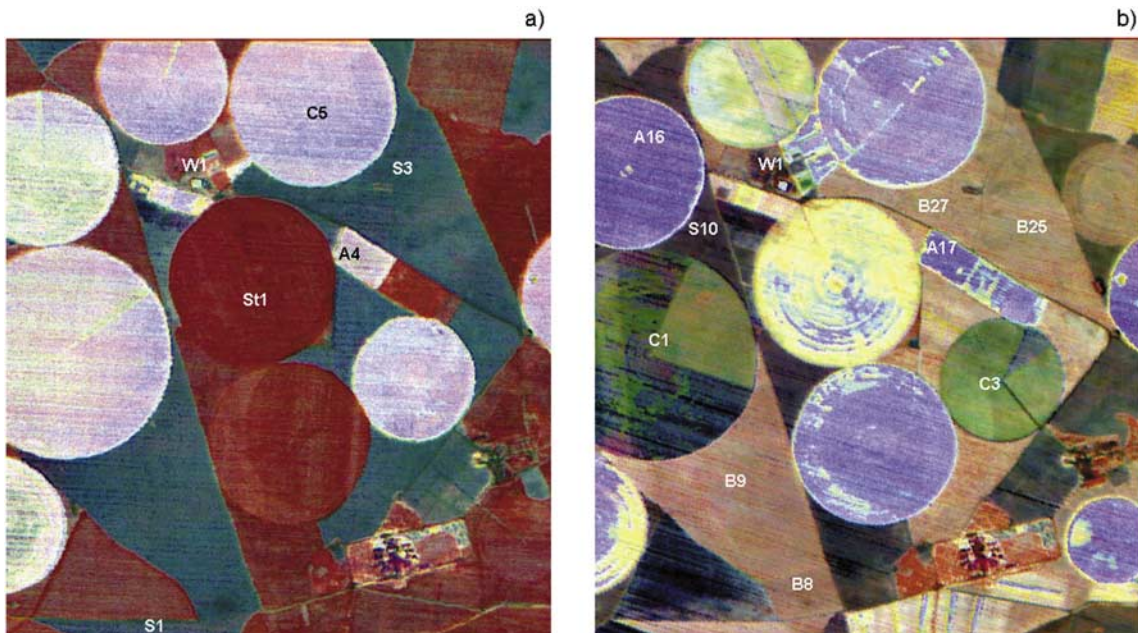

Figure 3. False color images of emissivity with channel 74 in red, channel 76 in green, and channel 77 in blue derived from line 1 of the DAIS flights on (a) August 11, 1998; and (b) June 3, 1999. Selected fields are indicated as in Figure 1.
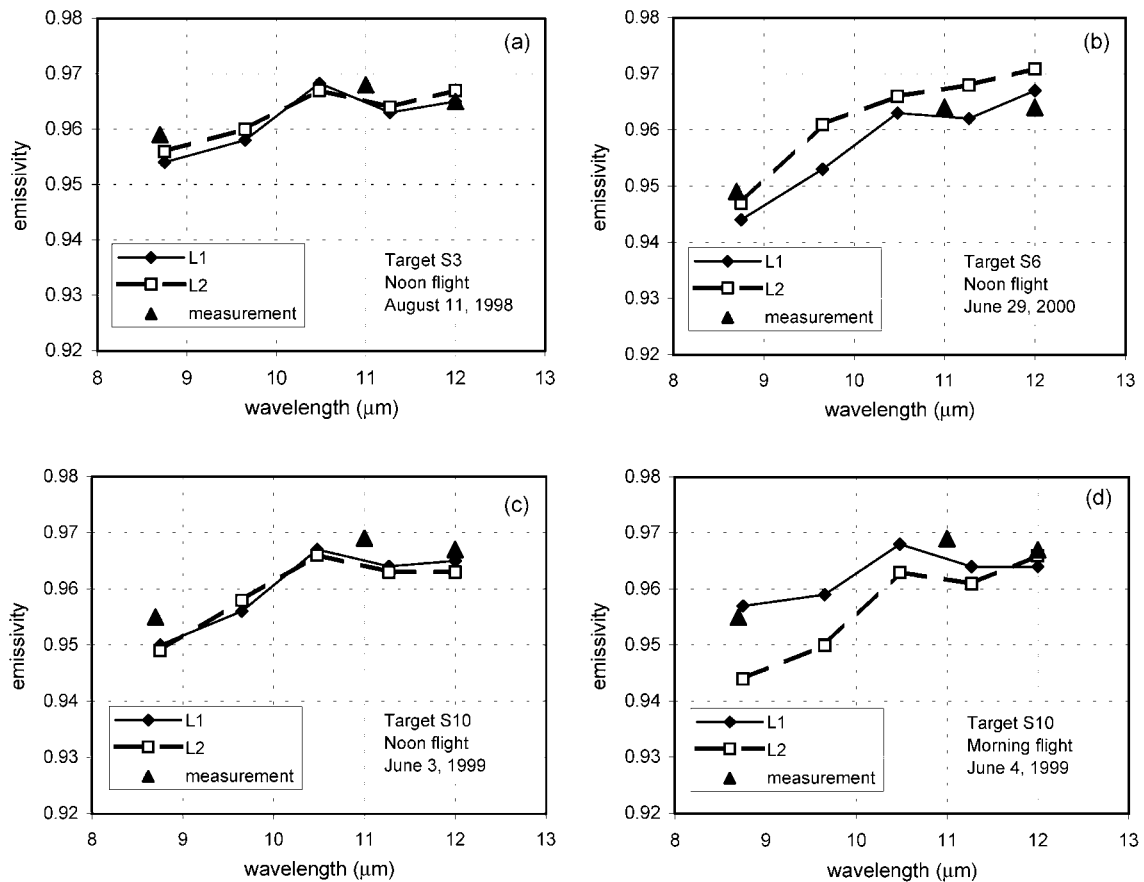
Figure 4. Emissivity spectra recovered with ANEM for bare soil: (a) S3, 1998. (b) S6, 2000. (c) S10, June 3, 1999. (d) S10, June 4 (morning), 1999. L1 is flight line 1; L2 is flight line 2. Solid triangles denote the field measurements made with CE 312 channels 2–4.

measurements [*Salisbury and D'Aria*, 1992]. Furthermore, Lambertian reflection does not hold for water surfaces, hence equation (3) is not strictly valid. The impact of this fact in the accuracy of the method is rather negligible due to the small observation angles of DAIS (up to ±26°) and the high value of water emissivity for such angles.

[22] In the ANEM algorithm, the maximum emissivity obtained pixel-by-pixel from equation (4) is used in equation (3), and the NEM algorithm is applied as usual to retrieve the surface temperatures and emissivity spectra. The key point of ANEM is to adjust the emissivity spectra and temperature obtained by NEM to match the maximum emissivity estimated from the vegetation cover. The accuracy of the retrieved temperatures and spectra depends on the difference between the actual and the calculated value of ε_{max}. According to our calculations, an emissivity difference of ±0.01 yields a variation in surface temperature of ±0.5 K (assuming a surface temperature of 300 K, midlatitude summer atmospheric profiles and wavelength range of 10–12 μm). The calculation of a reliable ε_{max} is facilitated by the relatively small variation of emissivity in the 10–12.5 μm region and its dependence on the vegetation cover.

5. Results and Discussion

[23] The ANEM algorithm was applied to all the scenes acquired in the DAISEX campaigns. For each scene, we

calculated one image of surface temperature and five images of emissivity in DAIS channels 74–78. As an example, Figure 1 shows images of surface temperature for line 1 of the noon flights in the three campaigns. Figure 2 shows emissivity images in channels 74 and 77 for the same scenes of Figure 1. In this section, the retrieved temperatures and emissivities are analyzed and discussed considering the main surface types in the area for the different years of the experiment. In 1998, there were irrigated alfalfa and corn crops with nearly full cover, bare soil and barley stubble. The area had more diversity in 1999, including irrigated plots with full cover of green vegetation (alfalfa, wheat and others), corn crops with very low vegetation cover, and fields of senescent and mature non-irrigated barley, as well as small plots of bare soil. In 2000, the main surfaces were fields of corn with medium vegetation cover, alfalfa (both harvested and full cover), barley stubble, and bare soil.

[24] In first place, the accuracy of the retrieved temperatures was tested with the coincident ground measurements of Table 3. The location of the measurement sites is shown in Figure 1. Table 5 shows the average and the standard deviation of the ANEM derived temperatures for arrays of 5 × 5 pixels centered at the site of the measurements, for each field, line and flight. The differences between the measured and the derived temperatures (ΔT) are also given. The results show a good performance of the ANEM algo-
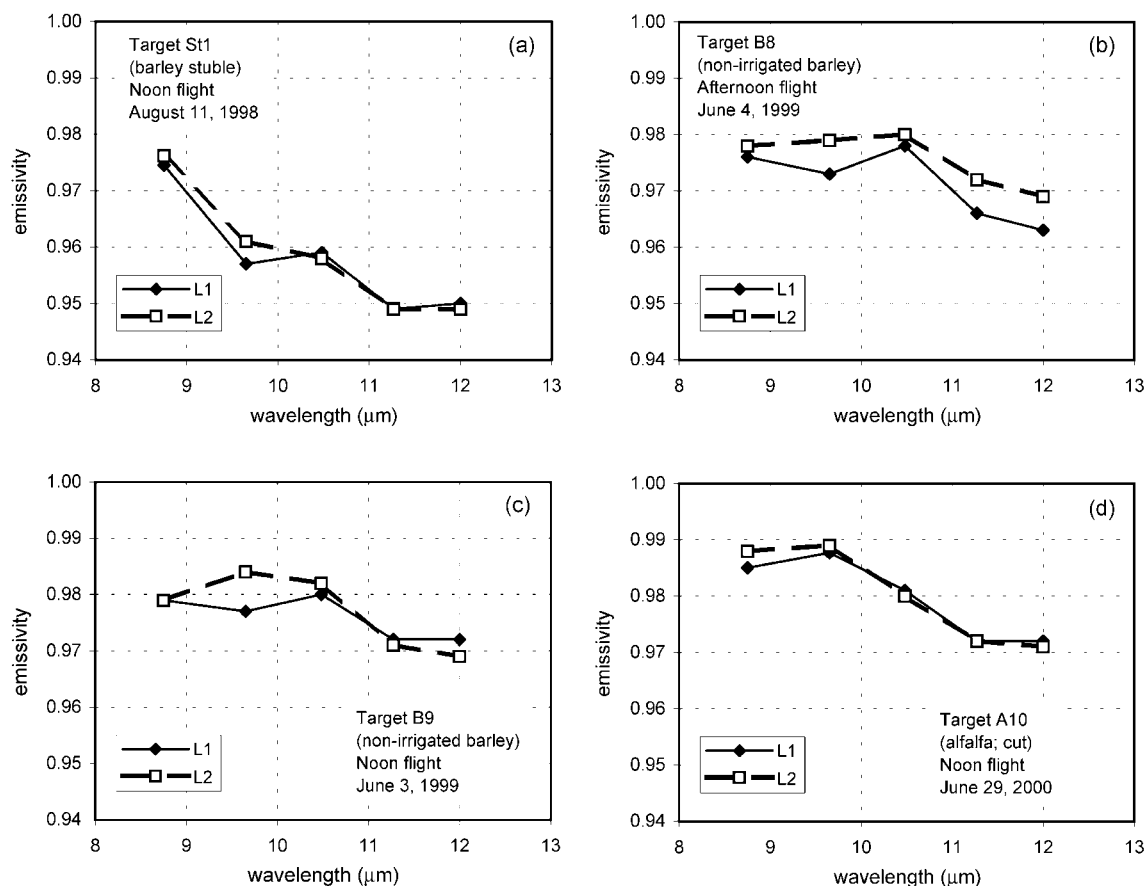
Figure 5. Emissivity spectra recovered with ANEM for senescent vegetation: (a) St1, 1998. (b) B8, June 4 (afternoon), 1999. (c) B9, June 3, 1999. (d) A10, 2000. L1 is flight line 1; L2 is flight line 2.

rithm, which agreed with the ground temperatures within ±1 K for most of the cases. Taking into account all the data of Table 5, the mean value and the standard deviation of the differences was −0.1 K and ±0.8 K, respectively.

[25] A similar analysis was performed with the temperatures derived from the NEM algorithm with a fixed emissivity input $\varepsilon_{NEM} = 0.97$. Taking together all the ground data, the difference ΔT yielded an average value of −0.7 K with a standard deviation of ±0.9 K. It is interesting to group the data by surface types and compare the results with ANEM, as shown in Table 6 where we give the average and standard deviation of ΔT for each group. According to these results, the ANEM algorithm provided nearly unbiased surface temperatures regardless the type of surface. For the bare soil sites, NEM and ANEM temperatures were nearly the same, since the actual maximum emissivity of the soils in the area was close to 0.97 (see Table 4). For the non-irrigated barley, green vegetation, and water surfaces, ε_{NEM} was too small compared with the actual maximum emissivity thus resulting in an overestimation of surface temperatures by 0.6 K, 1.4 K and 1.3 K, respectively.

[26] The emissivity images of Figure 2 show banding and noise effects (they are more evident in other scenes not shown), which suggest certain instrumental problems in the thermal part of DAIS. In order to check the stability of DAIS, we compared the emissivities retrieved in lines 1 and 2 of each flight, assuming that emissivity should not change

since they were acquired few minutes apart. For each channel and flight, Table 7 shows the average and the standard deviation of the difference between the emissivity retrieved in lines 1 and 2 for the whole study area. From this analysis, the 1998 flight yielded the smallest standard deviations for all channels, whereas the morning flight of June 4, 1999 had the largest. In all flights, channel 76 was the most stable with a mean standard deviation of ±0.007 (similar values for channels 75 and 77). Channel 78 was the most unstable, with standard deviations ranging from ±0.009 in 1998 to ±0.014 in the morning flight of 1999. Channel 74 showed somewhat smaller standard deviations (from ±0.007 to ±0.011). These deviations were attributed in part to stability problems of DAIS, and could not be removed by the vicarious calibration. As discussed in section 3.1, another possible source of error was the resampling of monochromatic radiance with the spectral response of the channels. This effect can yield an error in the retrieved emissivity of ±0.005 for DAIS channels 74−78 [*Richter and Coll*, 2002].

[27] Despite the problems discussed above, we analyzed the retrieved emissivities for the main surface types of the area. In addition to Figure 2, we show in Figure 3 false color composites of emissivity in channels 74 (red), 76 (green) and 77 (blue) for line 1 of the noon flights of 1998 and 1999. Such images are interesting in order to show the distribution of the different land cover types of the area and their change
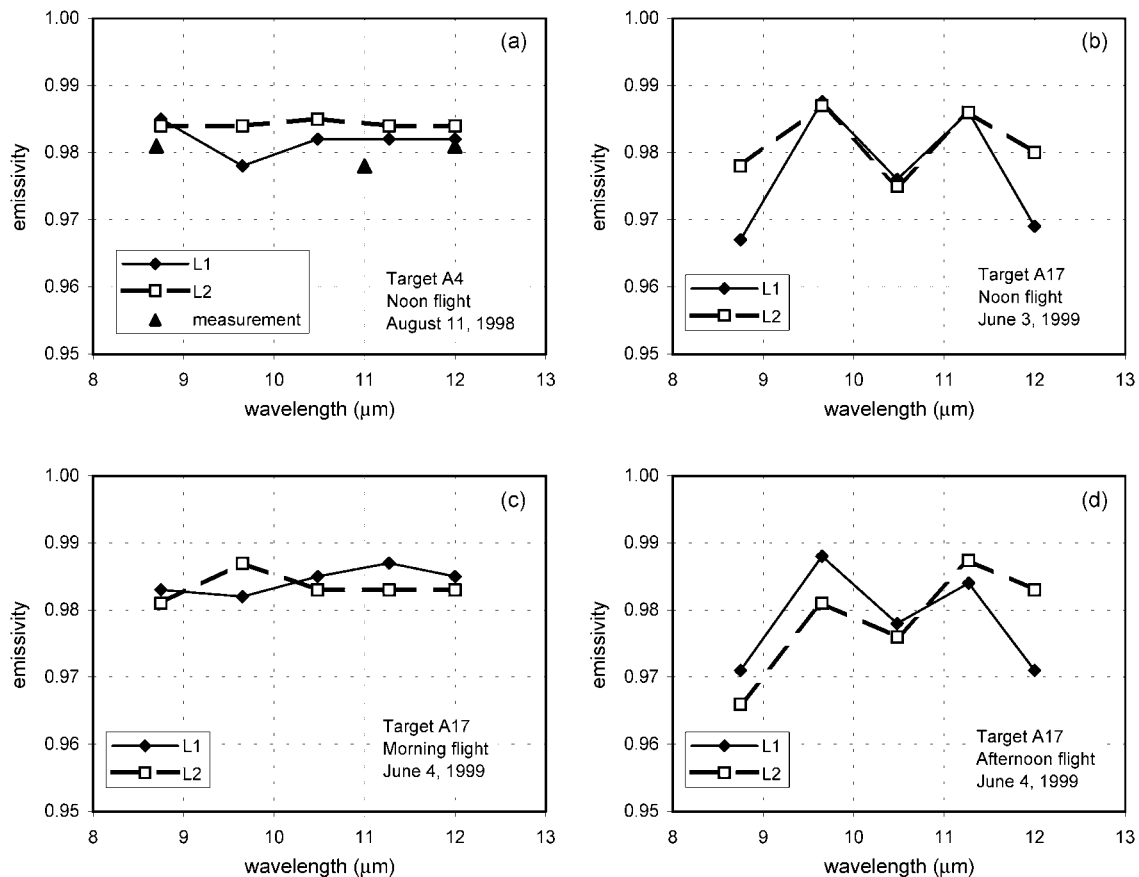
Figure 6. Emissivity spectra recovered with ANEM for alfalfa crops: (a) A4, 1998. (b) A17, June 3, 1999. (c) A17, June 4 (morning), 1999. (d) A17, June 4 (afternoon), 1999. L1 is flight line 1; L2 is flight line 2. Solid triangles denote the field measurements made with CE 312 channels 2–4.

with time. On the basis of Figures 2 and 3, a discussion of the results grouped by surface types follows.

5.1. Soils

[28] According to Figure 2, bare soils show low emissivity at channel 74 and relatively higher at channel 77. Consequently, soils appear in dark blue in the false color images of Figure 3. This is the typical "reststrahlen" effect of soils with absorption bands of quartz and biotite around 9 μm [*Salisbury and D'Aria*, 1992]. Figure 4 shows the retrieved spectra for several fields of bare soil in the three DAISEX campaigns. For comparison, we also plot the emissivity measurements for CE 312 channels 2–4 corresponding to these fields (Table 4). In general, there is good agreement between measured and recovered emissivities, with differences mostly within ±0.005. However, discrepancies up to 0.01 appear in some cases (e.g., Figure 4d). Such discrepancies were attributed to the instability of DAIS and were especially evident in the scenes of the 1999 morning flight.

5.2. Senescent Vegetation

[29] Different stages of senescent vegetation can be observed through the DAISEX campaigns. Barley had been recently harvested in 1998 and 2000, so we had fields of barley stubble and straw. According to Figure 2a, emissivity is higher for channel 74 than for channel 77, therefore

stubble appears in red in Figure 3a. The corresponding emissivity spectrum is shown in Figure 5a, where a decrease in emissivity of 0.025 from 9 to 12 μm is observed. It should be noted that, while bare soil and stubble show similar temperatures (see Figure 1a), the differences in their spectral emissivity signature makes them easily distinguishable. Similarly, a decrease of emissivity with wavelength is observed for non-irrigated barley in 1999, when the crop was mature and dry (Figures 5b and 5c), although the spectral contrast is smaller than for stubble. Such non-irrigated barley fields appear as light brown in Figure 3b. A similar behavior can be observed for the alfalfa field A10 in 2000 (Figure 5d), which was cut at the time of the flights. The observed decrease of emissivity with wavelength is typical for senescent vegetation [*Salisbury and D'Aria*, 1992]. This feature is useful to distinguish between bare soil and senescent vegetation with more accuracy than using visible and near infrared data alone [*French et al.*, 2000].

5.3. Alfalfa

[30] This irrigated crop had the highest fractional cover (>95%) during all campaigns, showing low temperatures (Figure 1) and high emissivities in all channels (Figure 2). Accordingly, alfalfa fields appear in white in the false color composites of emissivity (e.g., field A4 of Figure 3a). Figure 6a shows the emissivity spectra obtained for field A4 in 1998, which is in good agreement with the corresponding
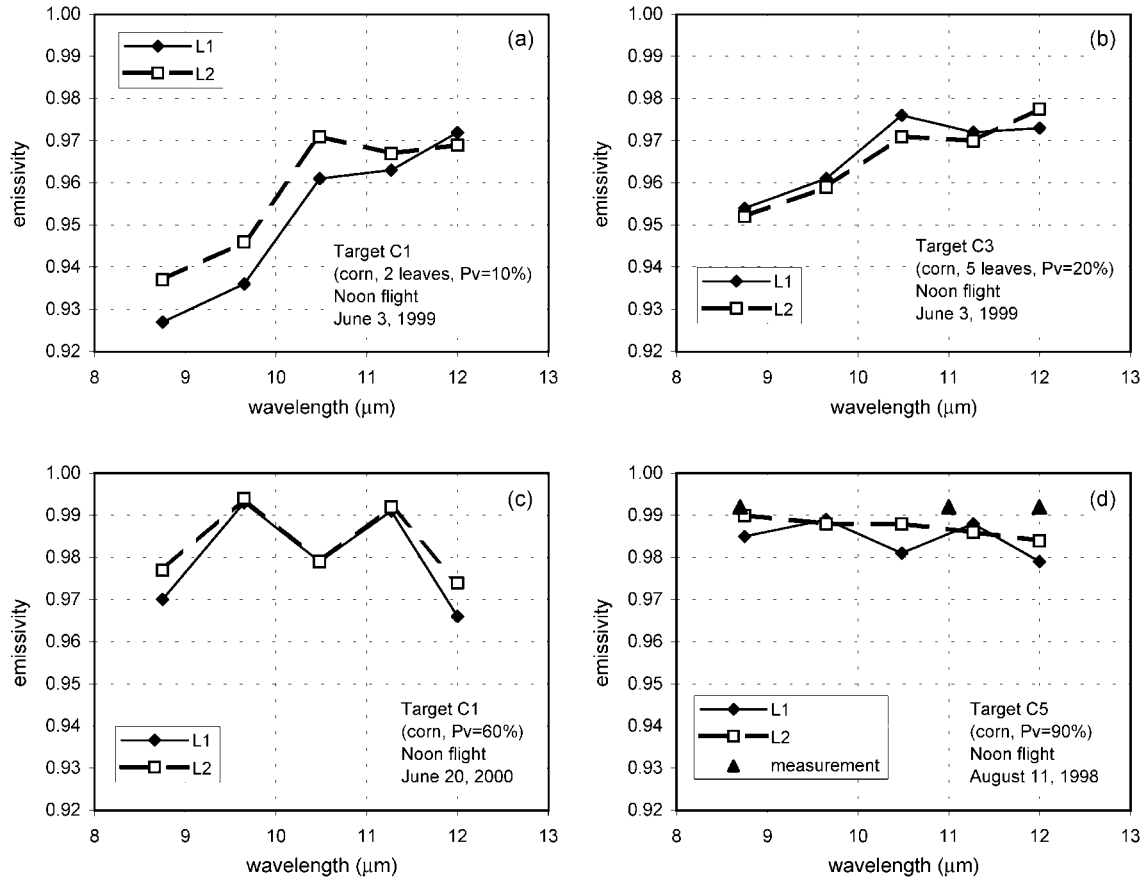
Figure 7. Emissivity spectra recovered with ANEM for corn crops: (a) C1, June 3, 1999. (b) C3, June 3, 1999. (c) C1, 2000. (d) C5, 1998. L1 is flight line 1; L2 is flight line 2. Solid triangles denote the field measurements made with CE 312 channels 2−4.

field measurements of Table 4. Figures 6b−6d show the results for the same field through the three flights of 1999. For certain lines and flights, the emissivity spectra yielded an average value of 0.980 with differences of ±0.01 between channels (Figures 6b and 6d). Similar "M-shaped" spectra were also observed for other surfaces of green vegetation with medium to high coverage (i.e., low temperatures), and are due to instrumental effects not totally solved by the vicarious calibration of the DAIS thermal channels. In the M-shaped spectrum, channel 77 typically resulted in higher emissivities; hence such cases appear in light blue in the false color composites (e.g., fields A16 and A17 in Figure 3b). In other cases (Figure 6c), the retrieved emissivities showed much less channel variations, more in accordance with the gray body behavior expected for high covers of green vegetation.

5.4. Corn

[31] Corn crops had different stages of development in the three DAISEX campaigns. In 1999, corn plants had two to five leaves and coverage of less than 20%. The emissivity spectra recovered for these fields were similar to that of bare soil (see Figures 7a and 7b). Corn was more developed in 2000, with vegetation cover of around 60%, whereas it attained nearly full cover (>90%) in 1998. Like alfalfa, these fields show low temperatures in Figure 1 and high emissivities in Figure 2, appearing in white or light blue in

Figure 3. Examples of emissivity spectra are shown in Figures 7c and 7d. Again, the M-shaped spectrum is observed with more or less amplitude depending on the line and the flight (Figure 7c). In other cases (Figure 7d), the retrieved emissivities showed small spectral variations, and a good agreement with the ground measurements.

5.5. Water

[32] The emissivities retrieved for the water body W1 were compared with the fresh water spectrum measured by *Salisbury and D'Aria* [1992], which was resampled to the DAIS channels. As stated in section 4, we used $\varepsilon_{max} = 0.99$ instead of equation (4) for applying the ANEM algorithm. Examples of results are shown in Figure 8. For all the flights and lines, the best results were obtained for channel 76 (maximum emissivity), with an average difference of 0.001, a standard deviation of ±0.001, and a maximum difference of 0.002. Channel 78 yielded the largest differences, with an average value of 0.002, a standard deviation of ±0.004, and a maximum difference of 0.011. Although W1 was used as a calibration point, the retrieved spectra showed relatively large discrepancies with respect to the measured spectra, especially for 1998 (Figure 8a). For the calibration, only 3×3 pixels in the center of the water body were used, whereas the spectra of Figure 8 represent the average values for all the water pixels. This fact, which should not be important for a homogeneous and nearly isothermal surface
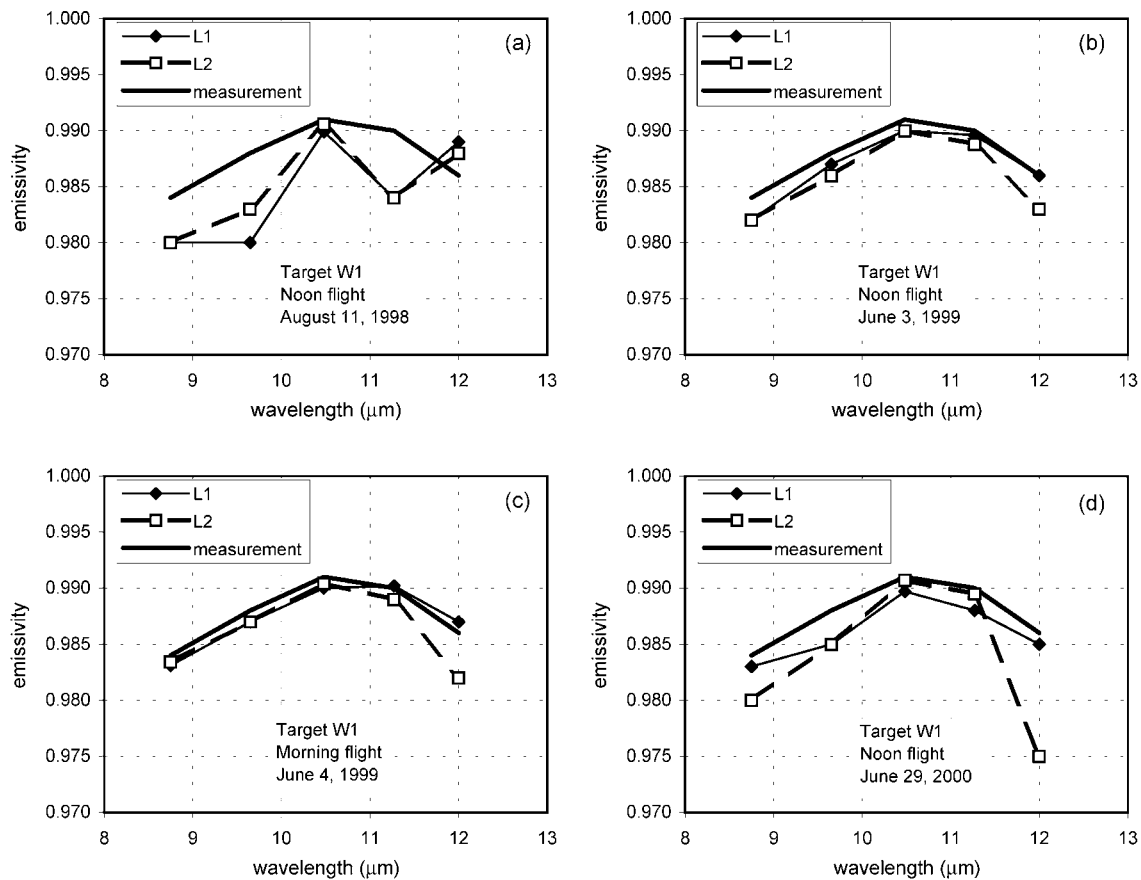
Figure 8. Emissivity spectra recovered with ANEM for the water body W1: (a) 1998. (b) June 3, 1999. (c) June 4 (morning), 1999. (d) 2000. L1 is flight line 1; L2 is flight line 2. The thick continuous line denotes the measurements of *Salisbury and D'Aria* [1992] for fresh water.

such as water, could make the difference in our case due to the instability of the DAIS instrument.

[33] A similar analysis was performed with the emissivities retrieved with the NEM algorithm with $\varepsilon_{NEM} = 0.97$. For all surface types, NEM emissivities showed nearly the same spectral variation as the corresponding ANEM emissivities. However, the NEM spectra were shifted so that their maximum emissivities always matched the fixed value of 0.97. While this was suitable for the soil sites in our study area, it underestimated the maximum emissivities derived from ANEM for other targets. In the case of green vegetation and water, the underestimation was about 0.02, and it was around 0.01 for senescent vegetation. These results are in accordance with the temperature overestimation shown by NEM in Table 6.

6. Conclusions

[34] An approach for the separation of emissivity and temperature from multispectral thermal infrared data was proposed in this paper. The Adjusted Normalized Emissivity Method (ANEM) uses visible and near infrared data to estimate pixel by pixel the maximum channel emissivity using the Vegetation Cover Method (VCM) [*Valor and Caselles*, 1996]. The pixel-dependent maximum emissivity is then used as the initial emissivity assumption in the NEM

[*Gillespie*, 1986]. The basis of ANEM is that maximum emissivities have a small variability and depend on the vegetation cover of the surface. By using an adjusted initial emissivity, the bias in the temperatures and emissivities retrieved by NEM can be reduced.

[35] The method was applied to airborne data recorded by DAIS during the three campaigns of the DAISEX project, which was carried out at the test site of Barrax, Spain in 1998–2000. Owing to the instrumental problems of the thermal infrared part of DAIS, a vicarious calibration was performed with ground measurements for two calibration targets (bare soil and water). In addition, at-sensor radiances were corrected for atmospheric effects with local, temporally coincident atmospheric profiles and the ATCOR4 code [*Richter*, 2000]. An accurate atmospheric correction is necessary in order to achieve reliable results in temperature-emissivity separation algorithms.

[36] A comparison between DAIS-retrieved and ground-measured temperatures and emissivities was performed for various fields. In terms of temperatures, the comparison yielded an agreement within ±0.8 K with nearly zero bias, regardless the type of surface. These results showed an improvement over the NEM algorithm with a fixed emissivity input, especially for vegetated fields. However, it should be noted that the Barrax test site does not contain pixels of high spectral contrast (bedrock) and maximum emissivities range from roughly 0.97 (soil) to 0.99 (green

vegetation). The performance of the algorithm in areas with higher emissivity variability will be tested in future studies.

[37] On the other hand, retrieved emissivities showed certain artifacts such as banding, noise and instabilities between consecutive flight lines. These effects were attributed to instrumental problems of DAIS, which could not be removed by the vicarious calibration. Channel resampling effects could generate considerable errors in the emissivity retrieval, depending on many factors such as surface temperatures, emissivities, bandwidth and spectral range [*Richter and Coll*, 2002]. Considering these limitations, the emissivities derived with ANEM agreed well with the available field data, with errors mostly within ±0.01. Furthermore, the potential of the emissivity spectra to discriminate between water, bare soil, senescent vegetation and green vegetation was shown. These encouraging results support the possibility of applying the ANEM algorithm to spaceborne instruments with multispectral channels in the visible/near infrared and thermal infrared.

Appendix A

[38] The effective emissivity of a heterogeneous and rough surface can be defined as [*Valor and Caselles*, 1996]

$$\varepsilon_j = \varepsilon_{vj}P_v + \varepsilon_{sj}(1 - P_v) + 4\langle d\varepsilon_j \rangle P_v(1 - P_v) \qquad (A1)$$

where ε_{vj} and ε_{sj} are respectively the vegetation and soil emissivities in channel j, P_v is the vegetation fractional cover, and $\langle d\varepsilon_j \rangle$ is a term accounting for the internal reflections between vegetation and soil, which depends on the structure of the surface (cavity term). The emissivity coefficients of equation (A1) were calculated for the DAIS thermal channels using the spectral library of *Salisbury and D'Aria* [1992]. For each channel, ε_{vj} was taken as the average for the green vegetation samples in the database, and ε_{sj} was taken as the average for soils and rocks. With the estimates of ε_{vj} and ε_{sj}, the cavity term was calculated for a wide variety of surface geometries, for which the average $\langle d\varepsilon_j \rangle$ was obtained. Using equation (A1) and the emissivity coefficients for DAIS, channel emissivities ε_j (j = 74−78) were modeled as a function of P_v. Then, the maximum channel emissivity, ε_{max}, was obtained in terms of P_v as

$$\varepsilon_{max} = 0.988 P_v + 0.964(1 - P_v) + 0.06 P_v(1 - P_v) \qquad (A2)$$

which is equation (4) in the text. The vegetation cover required in equation (A2) can be estimated from visible and near infrared data. We have used a reflectance linear mixture model with two components (soil and vegetation), and DAIS channels 10 (center at 0.654 μm, width of 0.022 μm) and 25 (center at 0.912 μm, width of 0.038 μm). These bands were selected to maximize the spectral contrast at the red edge for green vegetation. From the mixing model, P_v can be retrieved with the following relationship [*Valor and Caselles*, 1996]

$$P_v = \frac{\left(1 - \frac{i}{i_s}\right)}{\left(1 - \frac{i}{i_s}\right) - K\left(1 - \frac{i}{i_v}\right)} \qquad (A3)$$

where i is a vegetation index given by $i = (\rho_{25} - \rho_{10})/(\rho_{25} + \rho_{10})$ with ρ_{25} and ρ_{10} being the at-surface reflectances for channels 25 and 10, respectively; i_s and i_v are the minimum and maximum values for i in the image (corresponding to bare soil and green vegetation, respectively), and $K = (\rho_{25v} - \rho_{10v})/(\rho_{25s} - \rho_{10s})$, with ρ_{js} (ρ_{jv}) being the channel j reflectance for the pixels where i_s (i_v) were obtained.

References

Becker, F., and Z.-L. Li, Temperature-Independent spectral indices in thermal infrared bands, *Remote Sens. Environ.*, *32*, 17−33, 1990.

Becker, F., and Z.-L. Li, Surface temperature and emissivity at various scales: Definition, measurement and related problems, *Remote Sens. Rev.*, *12*, 225−253, 1995.

Berger, M., M. Rast, P. Wursteisen, E. Attema, J. Moreno, A. Müller, U. Beisl, R. Richter, M.-P. Stoll, F. Nerry, and M. Leroy, The DAISEX campaigns in support of a future land-surface-processes mission, *ESA Bull.*, *105*, 101−111, 2001.

Berk, A., G. P. Anderson, P. K. Acharya, J. H. Chetwynd, L. S. Bernstein, E. P. Shettle, M. W. Matthew, and S. M. Adler-Golden, *MODTRAN4 User's Manual*, Air Force Res. Lab., Space Vehicles Dir., Air Force Mater. Comm., Hascom Air Force Base, Mass., 1999.

Caselles, V., and J. A. Sobrino, Determination of frosts in orange groves from NOAA-9 AVHRR data, *Remote Sens. Environ.*, *29*, 135−146, 1989.

Caselles, V., E. Valor, C. Coll, and E. Rubio, Thermal band selection for the PRISM instrument: 1. Analysis of emissivity-temperature separation algorithms, *J. Geophys. Res.*, *102*, 11,145−11,164, 1997.

Coll, C., V. Caselles, E. Rubio, F. Sospedra, and E. Valor, Temperature and emissivity separation from calibrated data of the Digital Airborne Imaging Spectrometer, *Remote Sens. Environ.*, *76*, 250−259, 2001a.

Coll, C., V. Caselles, E. Rubio, F. Sospedra, and E. Valor, Analysis of thermal infrared data from the Digital Airborne Imaging Spectrometer, *Int. J. Remote Sens.*, *22*(18), 3703−3718, 2001b.

Dash, P., F. M. Göttsche, F. S. Olesen, and H. Fischer, Land surface temperature and emissivity estimation from passive sensor data: Theory and practice -current trends, *Int. J. Remote Sens.*, *23*(13), 2563−2594, 2002.

European Space Agency, Proceedings of the final results workshop on DAISEX (Digital Airborne Spectrometer Experiment), *Eur. Space Agency Spec. Publ.*, *499*, 278 pp., ESTEC, Noordwijk, Netherlands, 2001.

French, A. N., T. J. Schmugge, and W. P. Kustas, Discrimination of senescent vegetation using thermal emissivity contrast, *Remote Sens. Environ.*, *74*, 249−254, 2000.

Gillespie, A. R., Lithologic mapping of silicate rocks using TIMS, in *The TIMS Data Users' Workshop*, pp. 29−44, JPL Publ., Pasadena, Calif., 1986.

Gillespie, A. R., T. Matsunaga, S. Rokugawa, and S. J. Hook, Temperature and emissivity separation from Advanced Spaceborne Thermal Emission and Reflection Radiometer (ASTER) images, *IEEE Trans. Geosci. Remote Sens.*, *36*, 1113−1125, 1998.

Hausold, A., Geocoding methodology for imaging spectrometer data, *Eur. Space Agency Spec. Publ.*, *499*, 91−96, ESTEC, Noordwijk, Netherlands, 2001.

Kealy, P. S., and S. J. Hook, Separating emissivity and temperature in thermal infrared multispectral data: Implications for recovering land surface temperatures, *IEEE Trans. Geosci. Remote Sens.*, *31*, 1155−1164, 1993.

Li, Z.-L., F. Becker, M. P. Stoll, and Z. Wan, Evaluation of six methods for extracting relative emissivity spectra from thermal infrared images, *Remote Sens. Environ.*, *69*, 197−214, 1999.

Müller, A., P. Gege, and T. Cocks, The airborne imaging spectrometers used in DAISEX, *Eur. Space Agency Spec. Publ.*, *499*, 3−6, ESTEC, Noordwijk, Netherlands, 2001.

Richter, R., Atmospheric/topographic correction for wide FOV airborne imagery: Model ATCOR4, *DLR Rep. DLR-IB 564-04/00*, German Aerospace Center, Wessling, Germany, 2000.

Richter, R., and C. Coll, Band-pass resampling effects for the retrieval of surface emissivity, *Appl. Opt.*, *41*(18), 3523−3529, 2002.

Rubio, E., V. Caselles, and C. Badenas, Emissivity measurements of several soils and vegetation types in the $8-14$ µm waveband: Analysis of two field methods, *Remote Sens. Environ.*, *59*, 490–521, 1997.

Salisbury, J. W., and D. M. D'Aria, Emissivities of terrestrial materials in the $8-14$ µm atmospheric window, *Remote Sens. Environ.*, *42*, 83–106, 1992.

Sicard, M., P. R. Spyak, G. Brogniez, M. Legrand, N. K. Abuhassan, C. Pietras, and J.-P. Buis, Thermal-infrared field radiometer for vicarious cross-calibration: Characterization and comparison with other field instruments, *Opt. Eng.*, *38*, 345–356, 1999.

Strobl, P., and B. Zhukov, Recent developments in the $3-12$ µm radiometric calibration of the DAIS 7915, paper presented at first EARSeL Workshop on Imaging Spectroscopy, Zurich, Switzerland, 6–8 October , 1998.

Strobl, P., A. Müller, D. Schläpfer, and M. Schaepman, Laboratory calibration and in-flight validation of the Digital Airborne Imaging Spectrometer DAIS 7915, *Proc. SPIE*, *3071*, 225–235, 1997.

Valor, E., and V. Caselles, Mapping land surface emissivity from NDVI: Application to European, African and South American areas, *Remote Sens. Environ.*, *57*, 167–184, 1996.

_____

V. Caselles, C. Coll, R. Niclòs, and E. Valor, Department of Thermodynamics, Faculty of Physics, University of Valencia, C/Dr. Moliner, 50, 46100 Burjassot, Valencia, Spain. (cesar.coll@uv.es)